International Journal of Science and Engineering Applications
Volume 12-Issue 12, 18 - 24, 2023, ISSN:- 2319 - 7560
DOI:10.7753/IJSEA1212.1005

Unveiling the Promoted LSTM/YSZ Composite Anode for Direct Utilization of Hydrocarbon Fuels

Amin Nakhi
Nanotechnology and Advanced Materials Department
Materials and Energy Research Center
Karaj, Iran

Seyed Mostafa Nasrollahpour Shirvani
Department of Mechanical Engineering
Babol Noshirvani University of Technology
Babol, Iran

Amirmohammad Karimi
Department of Chemical Engineering
Azad University
Tehran, Iran

Mostafa Mobli*
Department of Mechanical Engineering
University of South Carolina
Columbia, United States

Abstract: The global quest for sustainable and diversified energy sources due to increased demand and environmental concerns has placed considerable emphasis on optimizing the efficiency of energy conversion devices. Solid oxide fuel cells (SOFCs) are known for their superior energy conversion capabilities utilizing hydrocarbons directly. Conventional SOFC anodes, typically composed of Ni/YSZ cermet, have drawbacks, such as susceptibility to coking and sulfur poisoning when using hydrocarbon fuels. Mixed ionic and electronic conductive (MIEC) materials, including $La_{0.4}Sr_{0.6}Ti_{1-x}Mn_xO_3$, have gained attention for their resistance to carbon and sulfur-related problems, as well as their thermal and redox stability. This study explores the electro-oxidation of methanol on a composite anode made of $La_{0.4}Sr_{0.6}Ti_{0.6}Mn_{0.4}O_{3-\delta}$ and yttria-stabilized zirconia. To enhance the electrode's performance, $LaFe_{0.6}Co_{0.4}O_3$ solutions, with various concentrations, are impregnated into the composite anode. Impedance spectroscopy measurements reveal improved performance, especially with the inclusion of ethylene glycol (EG), demonstrating lower electrode polarization resistance and enhanced catalytic activity. The X-ray diffraction analysis confirms the formation of LFC perovskite phases within the porous structure of the composite anode. The results indicate that the impregnation of LSTM/YSZ composite anodes with LFC solutions, particularly those with EG, enhances the methanol electro-oxidation reaction, making this composite a promising candidate for high-performance SOFC anodes. This research paves the way for more efficient and stable SOFCs, contributing to the sustainable energy landscape.

Keywords: solid oxide fuel cell, anode electrode, LSTM/YSZ, electrochemical impedance spectroscopy, methanol oxidation, LFC

1. INTRODUCTION

The increasing global demand for energy, coupled with the significant environmental consequences associated with traditional energy resources, has propelled the pursuit of sustainable and diverse energy sources [1-10]. A prominent focus in this undertaking revolves around augmenting the efficiency of energy conversion devices, particularly solid oxide fuel cells (SOFCs) [2, 11-14] and batteries [15-17]. SOFCs, distinguished for their exceptional energy conversion capabilities, generate electricity through electrochemical reactions involving gaseous fuels [12, 18-20]. Hydrogen stands as the primary fuel for SOFCs, mainly derived from the reformation of hydrocarbons. In contrast to other fuel cell varieties, SOFCs possess the distinct capacity to directly employ hydrocarbon fuels through internal reformation [21, 22]. Liquid hydrocarbons such as alcohols can be readily synthesized via industrial procedures and biomass sources [23, 24]. Among the various alcohol types, methanol is the simplest, characterized by its singular carbon atom in its molecular structure [25]. The absence of a robust C–C bond in methanol's composition notably streamlines the reformation process for its direct utilization within SOFCs [26-28]. Furthermore, methanol boasts a high hydrogen-to-carbon ratio, thereby yielding a substantial quantity of hydrogen molecules for the anode electrode in SOFCs.

In conventional SOFC configurations, the utilization of Ni/YSZ ($Zr_xY_{1-x}O_2$) cermet has been explored as a promising material for the anode electrode due to its numerous advantages, including low impedance in the presence of hydrogen and catalytic activity for methane steam reforming [29-33]. Nonetheless, this material is not without its drawbacks, notably exhibiting low redox stability and a high susceptibility to coking and sulfur poisoning when hydrocarbon fuels are employed [34-36]. Given the continued high cost of producing pure hydrogen, extensive research efforts have been directed toward the development of novel materials for the anode electrode in solid oxide fuel cells.

Materials that exhibit mixed ionic and electronic conduction (MIEC) have garnered considerable interest as potential electrode materials for SOFCs [37-42]. Among these ceramic anodes, including double perovskite materials like $Sr_2Mg_{1-x}Mn_xMoO_{6-\delta}$ [43-45], strontium titanate-based perovskites such as $(La,Sr)TiO_{3-\delta}$ [46, 47], and lanthanum chromate based perovskites like $(La,Sr)(Cr,Mn)O_{3-\delta}$ [38, 48, 49] have demonstrated promising characteristics for SOFC anodes. In particular, the $La_{0.4}Sr_{0.6}Ti_{1-x}Mn_xO_3$ material has garnered attention as a high-potential anode material. This interest stems from its remarkable resistance to carbon and sulfur-related issues, as well as its robustness in terms of redox and thermal cycling stability [50]. Fu et. al. [50] have explored the behavior of the $La_{0.4}Sr_{0.6}Ti_{1-x}Mn_xO_3$ anode when operated with wet hydrogen as the fuel. Remarkably, this anode achieved a maximum power density of approximately 0.365 W cm^{-2} at 0.7 V at 856 °C, which is comparable to the performance of Ni/YSZ-based anodes in wet H_2. Furthermore, $La_{0.4}Sr_{0.6}Ti_{1-x}Mn_xO_3$ remained chemically stable with YSZ, exhibiting relatively good stability in a reducing atmosphere at high temperatures [51]. However, there is room for

improvement in terms of the conductivity and catalytic activity of ceramic anodes like $La_{0.4}Sr_{0.6}Ti_{1-x}Mn_xO_3$ [52].

An effective strategy to enhance the performance of SOFC electrodes is the impregnation of nanoparticles composed of oxides or precious metals into the electrode structure [53, 54]. For instance, Kim et al. [55] investigated the stability of composite LSCM/YSZ anodes containing Pt, Pd, and Ni nanoparticles during operation with dry methane. Their findings revealed that Ni- and Pt-containing anodes experienced coking due to the deposition of a significant amount of carbon, which had a detrimental impact on electrode performance. Recently, $LaFe_{0.7}Co_{0.3}O_{3-\delta}$ (LFC) perovskite has emerged as a noteworthy material for symmetric electrodes in SOFCs [56]. LFC perovskite exhibits favorable electrocatalytic activity for both hydrogen oxidation and oxygen reduction reactions. For example, at 750 ºC, a symmetric LFC/$Sm_{0.2}Ce_{0.8}O_{1.9}$ (SDC) electrode achieved a power density of 0.291 W cm^{-2}. Additionally, Rostaghi Chalaki et. al. [38] demonstrated that the impregnation of LFC nanoparticles onto the LSCM/YSZ composite anode led to a substantial reduction in electrode polarization for direct oxidation of hydrocarbons.

This research delved into the electro-oxidation of methanol on the composite anode composed of $La_{0.4}Sr_{0.6}Ti_{0.6}Mn_{0.4}O_{3-\delta}$ (LSTM) and YSZ. To improve the electrode's performance, solutions of LFC at different concentrations were introduced into the LSTM/YSZ composite in a humidified environment with CH_3OH. Electrochemical measurements were employed to elucidate the mechanism of the methanol oxidation reaction on the enhanced anode. Furthermore, both unaltered and impregnated samples underwent thorough microstructural examination.

2. EXPERIMENTAL

To produce electrolyte pellets, a mixture containing 1 g of 8 mol % yttria-stabilized zirconia (YSZ) from Tosoh, Japan, and PVB binder was subjected to cold pressing. The resulting pellets were then sintered at a temperature of 1450 °C for a duration of 5 hours. The pellets attained a final diameter of approximately 18 mm and a thickness of 0.7 mm. Grinding was performed on the YSZ pellets to eliminate any surface impurities and achieve the desired roughness. The center of the YSZ pellets was coated with Pt paste, which served as the counter electrode with an area of 0.5 cm^2. Additionally, a reference electrode was applied in the form of a ring. Both the counter and reference electrodes were heated in air at 900 °C for 1 hour.

To create the anode electrode, a composite powder of LSTM and YSZ powder was prepared through a 10-hour roll-milling process in ethanol. The weight ratio of LSTM to YSZ was 1:1 to ensure a homogeneous mixture. The resulting powder was dried and combined with Ink Vehicle from Fuel Cell Material, USA, to form a suitable slurry of LSTM/YSZ. This slurry was then applied to the opposite side of the counter electrode and sintered in air at a temperature of 1200 °C for 3 hours. The resulting anode had a surface area of 0.5 cm^2 and a thickness of 30 µm after sintering. For impregnation, solutions of $LaFe_{0.6}Co_{0.4}O_3$ (LFC) were prepared in a specific order. Stoichiometric amounts of $La(NO_3)_3.6H_2O$, $Fe(NO_3)_3.9H_2O$, and $Co(NO_3)_2.6H_2O$ (all sourced from Merck, Germany) were dissolved in an aqueous solution in a 1:0.6:0.4:0 ratio. LFC solution concentrations of 0.2 M, 0.3 M, and 0.4 M were prepared. Ethylene glycol (EG) was added to the solution as a complexing agent in a 2.37:1 M ratio. A drop of LFC solutions with EG (E-LFC) and without EG (N-LFC), was carefully applied to the surface of the LSTM/YSZ composite anode. After impregnation, the electrode surface was gently wiped and dried in air. Subsequently, the impregnated cells were heated at 900 °C for 2 hours in an air environment.

Both LFC (0.3 M) solutions, N-LFC and E-LFC, were subjected to drying in an oven and subsequent calcination at 900 °C for 2 hours in an air environment, following the procedure described by Rostaghi Chalaki et. al. [38] for LFC calcination. The X-ray diffraction (XRD) analysis of the calcined LFC powders was performed using a Philips PW 1730 instrument at room temperature. Cu-Kα radiation (λ=1.5406 Å) was employed, and the scanning range covered 20°<2θ<80° with a step size of 0.02°. The microstructure of the impregnated LSTM/YSZ composite anodes was evaluated using a field emission scanning electron microscopy (FESEM) instrument, specifically the TESCAN MIRA3 model.

For the electrochemical measurements, a three-electrode configuration was adopted. Platinum paste was applied as a current collector on the surface of the anode electrode, and platinum wires were utilized as the current leads. Methanol gas served as the fuel, while the counter and reference electrodes were exposed to the surrounding atmosphere. Prior to commencing the electrochemical testing, all anodes were activated in methanol at 800 °C for one hour to stabilize the electro-catalytic activity of the electrode. The electrochemical impedance spectroscopy (EIS) of the anodes was recorded using an Autolab data analyzer (PGSTAT302) at open circuit potential (OCP), covering a frequency range from 0.01 Hz to 100 kHz. Z-view software was employed to calculate the electrode polarization resistance (R_E) and the electrode ohmic resistance (R_Ω).

3. RESULTS

3.1 Phase Characterization

Figure 1 illustrates the XRD outcomes obtained for the N-LFC and E-LFC powders after calcination in air at 900 °C. The XRD pattern of the N-LFC powder confirmed the presence of $LaFeO_3$, $LaCoO_3$, La_2O_3, and Fe_2O_3 oxides, but no LFC perovskite was detected. In contrast, the XRD pattern of the E-LFC calcined powder exhibited characteristics of the $LaFe_{0.6}Co_{0.4}O_3$ orthorhombic structure (JCPDS card no. 00-044-0361), with no additional Bragg peaks observed apart from those expected for the LFC perovskite. Therefore, it can be inferred that the LFC perovskite phase is likely formed within the porous structure of the LSTM/YSZ composite anode electrode after impregnation with the E-LFC solution.

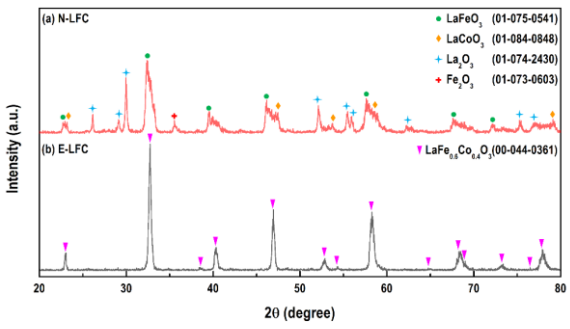

Figure 1. XRD patterns of N-LFC and E-LFC solutions calcined at 900 °C for 2 h in air.

3.2 Electrochemical Measurements

The impedance spectrum of the LSTM/YSZ composite anode under open circuit potential (OCP) and at a temperature of 800 °C in the presence of methanol is presented in Figure 2a. To investigate the impedance characteristics associated with methanol oxidation on the LSTM/YSZ composite anode, an equivalent circuit approach was employed. The impedance curves were analyzed using the $R_\Omega(RQ)_h(RQ)_m(RQ)_l$ equivalent circuit model, where R_Ω represents the ohmic resistance of the cell. Additionally, R_h, R_m, and R_l correspond to the electrode polarization resistances, which sum up to the total electrode polarization resistance ($R_E = R_h + R_m + R_l$). The model also incorporates Q_h, Q_m, and Q_l as constant phase elements at high-, medium-, and low-frequencies, respectively, as depicted in Figure 2b.

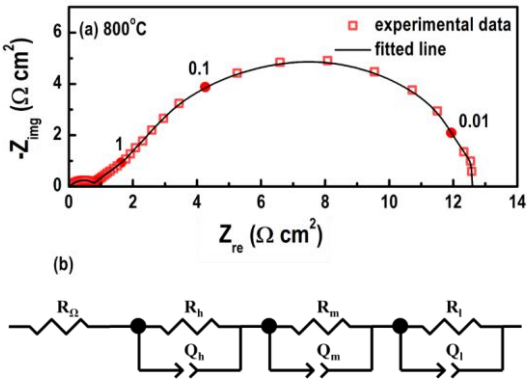

Figure 2. (a) LSTM/YSZ composite anode electrode polarization resistance at 800 °C in methanol. Points are experimental data and solid line is fitted data with the equivalent circuit $R_\Omega(RQ)_h(RQ)_m(RQ)_l$. Closed symbols mark the frequency points from 0.01 to 100 kHz at each frequency decade. (b) Equivalent circuit model for fitting the impedance spectra of the LSTM/YSZ composite anodes.

At a temperature of 750 °C, the electrode polarization resistance (R_E) for methanol oxidation was determined to be 17.81 Ω cm^2. As the temperature increased to 800 and 850 °C, the R_E values decreased to 12.62 and 8.30 Ω cm^2, respectively. To investigate the individual steps of the methanol oxidation reaction, the activation energy for each semicircle was determined. The activation energy for the high-, medium-, and low-frequency arcs was measured to be 1.08, -0.08, and 1.02 eV, respectively. This indicates that the high- and low-frequency arcs were thermally activated, while the medium-frequency arc experienced slight thermal deactivation.

Jiang et al. [57] conducted a study on the methane oxidation reaction occurring on the LSCM/YSZ composite anode in the presence of wet methane. They identified three distinct impedance arcs in their impedance spectra. These researchers attributed the high-frequency arc to the movement of charged species across the interface between LSCM and YSZ. In a separate investigation, a comparison was made between the $La_{0.4}Sr_{0.6}Ti_{1-x}Mn_xO_{3-\delta}$ anode and the $La_{0.4}Sr_{0.6}Ti_{1-x}Mn_xO_{3-\delta}$ /YSZ composite anode. It was observed that the composite anode exhibited a considerably smaller high-frequency arc when compared to the LSTM anode alone. This led to the conclusion that the composite anode possessed a significantly larger $La_{0.4}Sr_{0.6}Ti_{1-x}Mn_xO_{3-\delta}$ and YSZ interface area, thereby facilitating enhanced charge transfer [50]. Given the similarity of the high-frequency arc characteristics to those reported in references [50, 57], it can be inferred that the high-frequency arc corresponds to the transfer of charge species within the LSCM/YSZ composite anode.

Primdahl and Mogensen [58] conducted a study investigating the electrochemical oxidation of wet H_2 on a Ni/YSZ electrode in a three-electrode configuration at 1000 °C. They observed an impedance arc in the spectra with a peak frequency of approximately 1 Hz. This arc exhibited a small negative activation energy (-0.09 eV) and was attributed to gas conversion taking place on the surface of the Ni/YSZ anode electrode. Here, it should be noted that the composition of the fuel on the anode electrode is fundamentally different from that of the counter and reference electrode regions. The medium-frequency arc observed at 800 °C displayed a peak frequency of 0.55 Hz and an activation energy of -0.08 eV. By comparing this arc with the findings reported in references [50, 58], it can be inferred that the medium-frequency arc corresponds to the gas conversion occurring on the surface of the LSTM/YSZ composite anode electrode.

Jiang et al. [59] investigated the impedance spectra of Ni/YSZ anode in wet H_2 at 850 °C. They identified an impedance arc with a peak frequency of 0.02 Hz and an activation energy of 0.42 eV, which they attributed to hydrogen dissociative adsorption on Ni particles. Furthermore, it was observed that the low-frequency arc exhibited thermal activation. Considering these findings, it can be inferred that this particular arc is associated with the hydrogen dissociative adsorption occurring on the surface of the LSTM/YSZ composite anode electrode [59].

3.3 LFC Solutions Impregnation

The impact of incorporating different concentrations of N-LFC and E-LFC solutions on the performance of the LSTM/YSZ composite electrode at 800 °C in methanol is depicted in Figure 3. When the LSTM/YSZ composite electrode was impregnated with a 0.2 M E-LFC solution, the peak frequency of the high-frequency arc was over 10 kHz. Notably, all of this arc was shifted downwards, below the real axis on the Nyquist plot. On the other hand, when a 0.1 M N-LFC solution was used for impregnating the LSTM/YSZ composite anode electrode in methanol, a substantial reduction in R_E (from 12.62 to 6.97 Ω cm^2) was observed. Furthermore, with an increase in the concentration of N-LFC solution to 0.2 and 0.3 M, the R_E decreased further to 5.08 and 6.31 Ω cm^2, respectively. This decrease in R_E may be related to the promotion of catalytic activity or the enhancement of both ionic and electronic conduction within the LSTM/YSZ composite anode electrode facilitated by the impregnation of the LFC solution. In addition, the incorporation of E-LFC solutions at concentrations of 0.1, 0.2, and 0.3 M resulted in a decrease in the polarization resistance of the electrode to 4.45, 2.53, and 3.11 Ω cm^2, respectively. The remarkable enhancement achieved by the E-LFC solution can be attributed to the inclusion of EG in the N-LFC solution, leading to the formation of LFC. LFC exhibits superior catalytic activity when compared to $LaFeO_3$ and $LaCoO_3$, which explains the observed improvements.

The influence of N-LFC and E-LFC solution concentrations on the electrode polarization resistance and the arcs at high, medium, and low frequencies is depicted in Figure 4. The electrode polarization resistance of the LSTM/YSZ composite anode during the methanol electro-oxidation reaction exhibited a substantial decrease upon impregnation with both LFC solutions. This reduction in electrode polarization resistance can primarily be attributed to the decrease in resistance at medium and low frequencies. For the pure

International Journal of Science and Engineering Applications
Volume 12-Issue 12, 18 - 24, 2023, ISSN:- 2319 - 7560
DOI:10.7753/IJSEA1212.1005

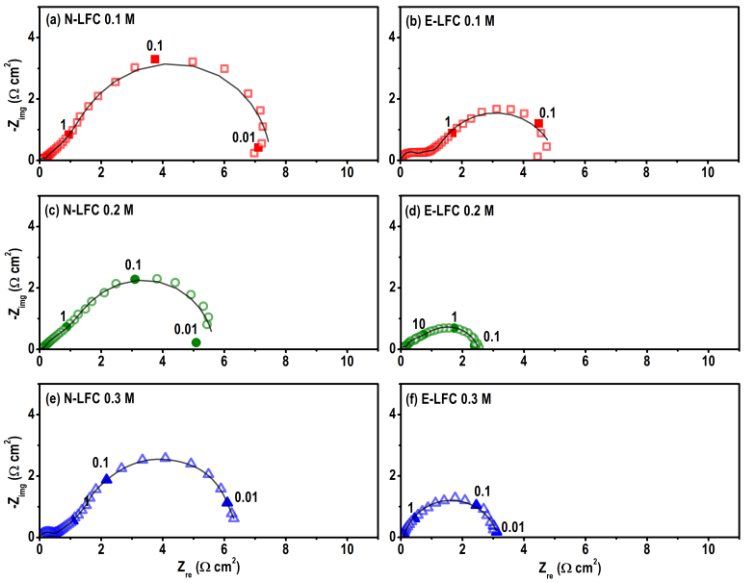

Figure 3. Impedance spectra of LSTM/YSZ composite anodes at different N-LFC and E-LFC solutions concentrations in methanol at 800 °C. Points are experimental data and solid lines are fitted data with the equivalent circuit. Closed symbols mark the frequency points from 0.01 Hz to 100 kHz at each frequency decade.

LSTM/YSZ composite anode at 800 °C, R_3 was 9.87 Ω cm^2, but it decreased to 2.93 and 1.2 Ω cm^2 upon impregnation with 0.2 M N-LFC and E-LFC solutions, respectively. The decline in electrode polarization resistance at low frequencies can be attributed to the promotion of the anode's catalytic activity for hydrogen adsorption resulting from LFC solutions impregnation. Notably, E-LFC solution demonstrated a greater reduction in R_3 compared to N-LFC solution, exceeding a two-fold decrease. Similarly, at medium frequencies, electrode polarization resistance decreased from 2.17 Ω cm^2 to 1.6 and 0.82 Ω cm^2 with 0.2 M N-LFC and E-LFC solution impregnation, respectively. Similar to the observations at high frequencies, E-LFC exhibited a more pronounced enhancement in electrode performance at medium frequencies compared to N-LFC solution, likely due to the impressive catalytic activity of LFC in methanol decomposition. Interestingly, electrode polarization resistance at high frequencies exhibited minimal changes upon N-LFC and E-LFC solutions impregnation, possibly indicating the ionic conductivity in the anode is affected significantly. However, the impregnation of 0.3 M LFC solutions led to an increase in electrode polarization resistance, potentially due to a non-uniform distribution of nanoparticles within the LSTM/YSZ porous backbone.

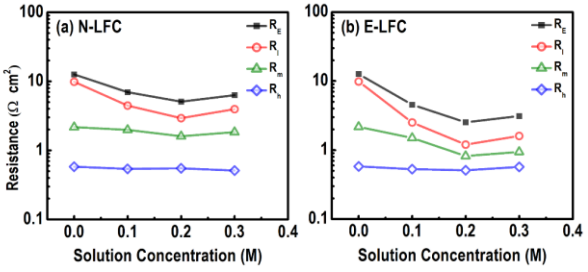

Figure 4. The effect of N-LFC and E-LFC solutions concentration on R_h, R_m, R_l, and R_E of LSTM/YSZ composite anode in methanol. Closed points are experimental data and open points are fitting results.

The SEM micrographs presented in Figure 5 illustrate the LSTM/YSZ composite anode electrode before and after impregnation with 0.2 M N-LFC and E-LFC solutions. Upon examination, it is evident that the impregnation of LFC solutions resulted in the formation of nanoparticles on the LSTM/YSZ composite anode electrode. The size of the LFC particles was determined using Digimizer software, with an average size of approximately 86 nm observed for the 0.2 M E-LFC solution. Notably, the impregnation of E-LFC solution exhibited better nanoparticle formation compared to N-LFC solution. As mentioned previously, the LSTM/YSZ composite anodes impregnated with 0.2 M E-LFC solution demonstrated lower R_E compared to other solutions. Therefore, the superior performance of the 0.2 M E-LFC solution can be attributed to the uniform distribution of LFC nanoparticles formed within the porous structure of the LSTM/YSZ anode.

4. CONCLUSION

In conclusion, the LSTM/YSZ composite anode exhibited a significant electrode polarization resistance during methanol oxidation at 800 °C. Analysis of the impedance spectra using an equivalent circuit revealed that the electro-oxidation of methanol on the LSTM/YSZ composite anode electrode is governed by at least three distinct electrode processes. These processes involve charge transfer at high frequencies, gas conversion at medium frequencies, and hydrogen dissociative adsorption on the LSTM/YSZ composite anode electrode at low frequencies. Notably, the impregnation of LFC solutions led to a substantial reduction in the polarization resistance of the LSTM/YSZ composite electrode. This improvement can be attributed to the presence of LFC nanoparticles, which enhance the electro-catalytic properties of the LSTM/YSZ composite anode by facilitating the processes of methanol decomposition and hydrogen adsorption. Furthermore, the reduction in electrode polarization resistance was enhanced with the concentration of 0.2 M LFC solutions. However, an increase in electrode polarization resistance was observed with the impregnation of 0.3 M LFC solutions, possibly due to the non-uniform distribution of LFC nanoparticles within the porous backbone of the LSTM/YSZ composite anode.

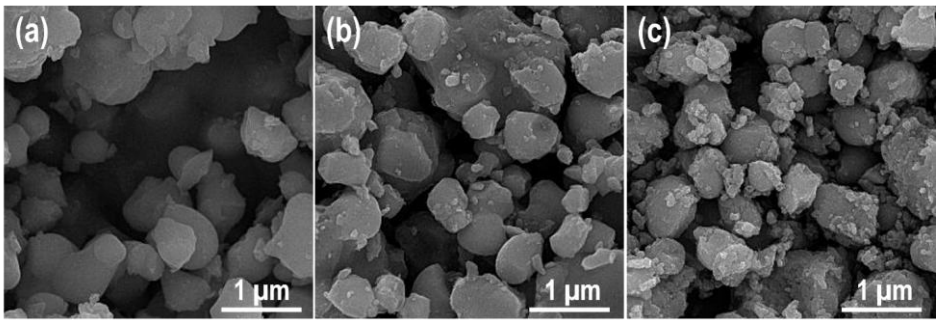

Figure 5. Field emission scanning electron microscopy (FESEM) images of LSTM/YSZ composite anode electrode, (a) before, and after impregnation with 0.2 M of (b) N-LFC and (c) E-LFC solutions.

5. ACKNOWLEDGMENTS

The author would like to thank the Nanotechnology and Advanced Materials Department at the Materials and Energy Research Center. This study did not receive funding from any government or private agency.

6. REFERENCES

1. Taghavi, H., Liquid Cooling System for a High Power, Medium Frequency, and Medium Voltage Isolated Power Converter. 2023, University of South Carolina: United States -- South Carolina. p. 74.

2. Soltanizade, A., et al., Temperature dependency of activity of nano-catalysts on La 0.6 Sr 0.4 Co 0.2 Fe 0.8 O 3− δ cathode of solid oxide fuel cells. Journal of Applied Electrochemistry, 2019. 49: p. 1113-1122.

3. Taghavi, H., A. El Shafei, and A. Nasiri. Liquid Cooling System for a High Power, Medium Frequency, and Medium Voltage Isolated Power Converter. in 2023 12th International Conference on Renewable Energy Research and Applications (ICRERA). 2023. IEEE.

4. Rajabi, R., et al., Insights into Chemical and Electrochemical Interactions between Zn Anode and Electrolytes in Aqueous Zn− ion Batteries. Journal of The Electrochemical Society, 2022. 169(11): p. 110536.

5. Taghavi, M., et al., Developing a model to predict the start of combustion in HCCI engine using ANN-GA approach. Energy Conversion and Management, 2019. 195: p. 57-69.

6. Taghavi, M. and L.P. Perera. Data Driven Digital Twin Applications Towards Green Ship Operations. in International Conference on Offshore Mechanics and Arctic Engineering. 2022. American Society of Mechanical Engineers.

7. Rajabi, R., S. Sun, and K. Huang. Performance Comparison of Three Polymer Electrolytes for Zinc Ion Batteries. in 243rd ECS Meeting with the 18th International Symposium on Solid Oxide Fuel Cells (SOFC-XVIII). 2023. ECS.

8. Bhuvela, P., H. Taghavi, and A. Nasiri. Design Methodology for a Medium Voltage Single Stage LLC Resonant Solar PV Inverter. in 2023 12th International Conference on Renewable Energy Research and Applications (ICRERA). 2023. IEEE.

9. Taghavi, M. and L.P. Perera. Multiple Model Adaptive Estimation Coupled With Nonlinear Function Approximation and Gaussian Mixture Models for Predicting Fuel Consumption in Marine Engines. in International Conference on Offshore Mechanics and Arctic Engineering. 2023. American Society of Mechanical Engineers.

10. Shirvani, S.M.N., et al., Optimal design of a composite sandwich panel with a hexagonal honeycomb core for aerospace applications. Iranian Journal of Science and Technology, Transactions of Mechanical Engineering, 2023. 47(2): p. 557-568.

11. Fan, L., et al., Nanomaterials and technologies for low temperature solid oxide fuel cells: recent advances, challenges and opportunities. Nano Energy, 2018. 45: p. 148-176.

12. Dizaj, R.B. and N. Sabahi, Optimizing LSM-LSF composite cathodes for enhanced solid oxide fuel cell performance: Material engineering and electrochemical insights. 2023.

13. Aminnia, N., et al., Three-dimensional CFD-DEM simulation of raceway transport phenomena in a blast furnace. Fuel, 2023. 334: p. 126574.

14. Aminnia, N., et al., Modeling of Two-Phase flow in the Cathode Gas Diffusion Layer to Investigate Its Effects on a PEM Fuel Cell.

15. Rajabi, R., et al. PERFORMANCE COMPARISON OF BATTERY THERMAL MANAGEMENT SYSTEMS BASED ON NUMERICAL SIMULATION. in ASTFE Digital Library. 2023. Begel House Inc.

16. Jeena, M., et al., A siloxane-incorporated copolymer as an in situ cross-linkable binder for high performance silicon anodes in Li-ion batteries. Nanoscale, 2016. 8(17): p. 9245-9253.

17. Raghu, S., et al. *Performance Comparison of Thermal Management Systems for Battery Packs Based on*

Numerical Simulation. in *Heat Transfer Summer Conference*. 2023. American Society of Mechanical Engineers.

18. Lee, K.T. and E.D. Wachsman, Role of nanostructures on SOFC performance at reduced temperatures. Mrs Bulletin, 2014. 39(9): p. 783-791.

19. Babazadeh Dizaj, R., DEVELOPMENT OF LSF-BASED DUAL-PHASE CATHODES FOR INTERMEDIATE TEMPERATURE SOLID OXIDE FUEL CELLS. 2022, Middle East Technical University.

20. Aminnia, N., A.A. Estupinan Donoso, and B. Peters, Developing a DEM-Coupled OpenFOAM solver for multiphysics simulation of additive manufacturing process. Scipedia. com, 2022.

21. Ge, X.M., et al., Solid oxide fuel cell anode materials for direct hydrocarbon utilization. Advanced Energy Materials, 2012. 2(10): p. 1156-1181.

22. Aminnia, N., CFD-XDEM coupling approach towards melt pool simulations of selective laser melting. 2023.

23. Atkinson, A., et al., Advanced anodes for high-temperature fuel cells. Nature materials, 2004. 3(1): p. 17-27.

24. Sun, R., et al., Crystallization Behavior and Luminescence of Inkjet Printing CH3NH3PbBr3. Crystal Research and Technology, 2021. 56(8): p. 2100004.

25. Li, H., et al. C2H6 Dehydrogenation and Electrical Power Production in a Protonic Conducting Fuel Cell with in-Situ Exsolved Metal Nanoparticle Catalyst. in Electrochemical Society Meeting Abstracts 239. 2021. The Electrochemical Society, Inc.

26. Sá, S., et al., Catalysts for methanol steam reforming—A review. Applied Catalysis B: Environmental, 2010. 99(1-2): p. 43-57.

27. Du, Y., et al., Preparation and thermoelectric properties of graphite/poly (3, 4-ethyenedioxythiophene) nanocomposites. Energies, 2018. 11(10): p. 2849.

28. Estupinan Donoso, A.A., et al., On the Reduction of Computational Costs for Tungsten Powder Bed Processes. 2022.

29. McIntosh, S. and R.J. Gorte, Direct hydrocarbon solid oxide fuel cells. Chemical reviews, 2004. 104(10): p. 4845-4866.

30. Jia-Yue, X., et al., Growth and characterization of all-inorganic perovskite CsPbBr3 crystal by a traveling zone melting method. Journal of Inorganic Materials, 2018. 33(11): p. 1253-1258.

31. Wang, M., et al., Nanostructured carbon as highly efficient and stable anodes for ethylene production and power generation in protonic ceramic electrochemical cells. Carbon, 2022. 199: p. 379-386.

32. Wang, W., et al., Improving the performance for direct electrolysis of CO 2 in solid oxide electrolysis cells with a Sr 1.9 Fe 1.5 Mo 0.5 O 6− δ electrode via infiltration of Pr 6 O 11 nanoparticles. Journal of Materials Chemistry A, 2023. 11(16): p. 9039-9048.

33. Aminnia, N., A.A. Estupinan Donoso, and B. Peters, CFD-DEM simulation of melt pool formation and evolution in powder bed fusion process. 2022.

34. Su, C., et al., Progress and prospects in symmetrical solid oxide fuel cells with two identical electrodes. Advanced Energy Materials, 2015. 5(14): p. 1500188.

35. Wang, M., et al., Improved Solid-State Reaction Method for Scaled-Up Synthesis of Ceramic Proton-Conducting Electrolyte Materials. ACS Applied Energy Materials, 2023. 6(15): p. 8316-8326.

36. Aminnia, N., B. Peters, and A.A. ESTUPINAN, Multi-Scale Modeling of Melt Pool Formation and Solidification in Powder Bed Fusion: A Fully Coupled Computational Fluid Dynamics-Extended Discrete Element Method Approach. Available at SSRN 4502227.

37. Yang, G., et al., Tuning Ionic Conductivity in Fluorite Gd-Doped CeO2-Bixbyite RE2O3 (RE= Y and Sm) Multilayer Thin Films by Controlling Interfacial Strain. ACS Applied Electronic Materials, 2023. 5(8): p. 4556-4563.

38. Rostaghi Chalaki, H., et al., LaFe 0.6 Co 0.4 O 3 promoted LSCM/YSZ anode for direct utilization of methanol in solid oxide fuel cells. Ionics, 2020. 26: p. 1011-1018.

39. Burnwal, S.K., S. Bharadwaj, and P. Kistaiah, Review on MIEC cathode materials for solid oxide fuel cells. Journal of Molecular and Engineering Materials, 2016. 4(02): p. 1630001.

40. Park, K.-Y., et al. A Highly Performing Electrode with in-Situ Exsolved Nanoparticles for Direct Electrolysis of CO2. in Electrochemical Society Meeting Abstracts 242. 2022. The Electrochemical Society, Inc.

41. Wang, W., et al. Rational Identification of Doping Strategy to Achieve a Highly Conductive and Reliable Protonic Electrolyte for Electrochemical Cells. in Electrochemical Society Meeting Abstracts 239. 2021. The Electrochemical Society, Inc.

42. mahmoodreza Hashemi, S., N. Aminnia, and S. Derakhshan, Optimization Design of Pumps as Turbines (PATs) Arrays in a Water Distribution Network Aiming Energy Recovery.

43. Huang, Y.-H., et al., Double perovskites as anode materials for solid-oxide fuel cells. Science, 2006. 312(5771): p. 254-257.

44. Li, H., et al., Improved cell performance and sulphur tolerance using A-site substituted Sr2Fe1. 4Ni0. 1Mo0. 5O6–δ anodes for solid-oxide fuel cells. Clean Energy, 2023. 7(1): p. 70-83.

45. Li, H., et al. A-Site Doping Effect on the Performance of Sr2Fe1. 4 Ni0. 1Mo0. 5O6-Δ Anodes for SOFCs. in Electrochemical Society Meeting Abstracts 242. 2022. The Electrochemical Society, Inc.

46. Marina, O.A., N.L. Canfield, and J.W. Stevenson, Thermal, electrical, and electrocatalytical properties of lanthanum-doped strontium titanate. Solid State Ionics, 2002. 149(1-2): p. 21-28.

47. Lin, J., et al., Atmospheric plasma spraying to fabricate metal-supported solid oxide fuel cells with open-channel porous metal support. Journal of the American Ceramic Society, 2023. 106(1): p. 68-78.

48. Li, H., et al., Unlocking the Potential of A-Site Ca-Doped LaCo0. 2Fe0. 8O3− δ: A Redox-Stable Cathode Material Enabling High Current Density in Direct CO2 Electrolysis. ACS Applied Materials & Interfaces, 2023. 15(37): p. 43732-43744.

49. Park, K.-Y., et al., High-performance Ruddlesden–Popper perovskite oxide with in situ exsolved nanoparticles for direct CO 2 electrolysis. Journal of Materials Chemistry A, 2023. 11(39): p. 21354-21364.

50. Fu, Q., F. Tietz, and D. Stöver, La0. 4Sr0. 6Ti1− x Mn x O3− δ perovskites as anode materials for solid oxide fuel cells. Journal of the Electrochemical Society, 2006. 153(4): p. D74.

51. Kim, J.H., et al., Investigation of microstructural and electrochemical properties of impregnated (La, Sr)(Ti, Mn) O3±δ as a potential anode material in high-temperature solid oxide fuel cells. Chemistry of Materials, 2011. 23(17): p. 3841-3847.

52. Fowler, D.E., et al., Decreasing the polarization resistance of (La, Sr) CrO3− δ solid oxide fuel cell anodes by combined Fe and Ru substitution. Chemistry of Materials, 2015. 27(10): p. 3683-3693.

53. Chalaki, H.R., et al. The Effect of Impregnation of Ceramic Nano-particles on the Performance of LSCM/YSZ Anode Electrode of Solid Oxide Fuel Cell. in 5th International Conference on Materials Engineering and Metallurgy. 2016.

54. Ye, Y., et al., Pd-promoted La0. 75Sr0. 25Cr0. 5Mn0. 5O3/YSZ composite anodes for direct utilization of methane in SOFCs. Journal of the Electrochemical Society, 2008. 155(8): p. B811.

55. Kim, J.-S., et al., A study of the methane tolerance of LSCM–YSZ composite anodes with Pt, Ni, Pd and ceria catalysts. Scripta Materialia, 2011. 65(2): p. 90-95.

56. Shen, J., et al., Impregnated LaCo0. 3Fe0. 67Pd0. 03O3-δ as a promising electrocatalyst for “symmetrical” intermediate-temperature solid oxide fuel cells. Journal of Power Sources, 2016. 306: p. 92-99.

57. Jiang, S.P., et al., (La0. 75Sr0. 25)(Cr0. 5Mn0. 5) O3/YSZ composite anodes for methane oxidation reaction in solid oxide fuel cells. Solid State Ionics, 2006. 177(1-2): p. 149-157.

58. Primdahl, S. and M. Mogensen, Gas conversion impedance: a test geometry effect in characterization of solid oxide fuel cell anodes. Journal of the electrochemical Society, 1998. 145(7): p. 2431.

59. Jiang, S., W. Wang, and Y. Zhen, Performance and electrode behaviour of nano-YSZ impregnated nickel anodes used in solid oxide fuel cells. Journal of power sources, 2005. 147(1-2): p. 1-7.